SUPPORTING INFORMATION

Ammonium-Preintercalated Layered Manganese Oxide with Single-Phase Intercalation Chemistry and Enhanced Two-Electron Reaction in Aqueous Zinc-Ion Batteries

Tzu-Ho Wu, Jian-Xue Huang, Syu-Jin Liao*

Department of Chemical and Materials Engineering, National Yunlin University of Science and Technology, Yunlin 64002, Taiwan. E-mail: wutzu@yuntech.edu.tw

1. Experimental Procedures

Chemicals.

Potassium permanganate ($KMnO_4$, 99%), potassium hydroxide (KOH, 85%), manganese(II) chloride ($MnCl_2$, 99%), ammonium persulfate ($(NH_4)_2S_2O_8$, 98%), ammonia solution ($NH_3 \cdot H_2O$, 28-30%), tetramethylammonium hydroxide (TMAOH, 98%), zinc sulfate heptahydrate ($ZnSO_4 \cdot 7H_2O$, 99%), manganese(II) sulfate monohydrate ($MnSO_4 \cdot H_2O$, 99%), and N-methyl-2-pyrrolidone (NMP, 99%) were purchased from Sigma-Aldrich and used as received. Zinc foil (99.98%, thickness = 0.25 mm), Super P (99%), and poly(vinylidene difluoride) (PVDF, 99%) were purchased from Alfa Aesar. CR2032 Coin-type cells, carbon paper substrates (GDS180S, thickness = 0.18 mm), glass fiber separator (GF6) were purchased from JuChen, CeTech, and Whatman, respectively.

Synthesis of K-MO.

The K-MO sample was synthesized via a one-step hydrothermal method from a $KMnO_4$–$MnCl_2$–KOH mixture. The precursor solution was firstly prepared by successively adding 263 mg of $KMnO_4$ and 56.1 g of KOH into 46.67 mL of deionized water under magnetic stirring. Then, 3.33 mL of 1 M $MnCl_2$ aqueous solution was introduced into the precursor solution under magnetic stirring for 3 h. Next, the mixed solution was transferred to a Teflon-lined stainless autoclave for the hydrothermal reaction at 175 ^oC for 48 h. The resulting precipitate was thoroughly washed with deionized water to remove KOH residue. After drying at 60 ^oC overnight, the K-MO powder sample was obtained.

Synthesis of NH_4-MO and TMA-MO

To prepare NH_4-MO (or TMA-MO), as-received K-MO was treated to remove the preintercalated K^+ ions and subsequently insert NH_4^+ (or TMA^+) ions. Typically, 400 mg of as-received K-MO was dispersed into 100 mL of 0.5 M $(NH_4)_2S_2O_8$ aqueous solution. The mixture was stirred and maintained at 60 ^oC for 12 h. Then, the solid precipitate was thoroughly washed with deionized water until the effluent became neutral. The black powder can be collected after drying at 60 ^oC. Subsequently, 200 mg of the obtained black powder was dispersed into 50 mL of 2.5 M $NH_3 \cdot H_2O$ (or TMAOH) aqueous solution. The reaction was maintained at 60 ^oC for 72 h under magnetic stirring. After thoroughly washing with deionized water and drying at 60 ^oC, the NH_4-MO (or TMA-MO) powder sample was collected.

Materials characterization.

X-ray diffraction (XRD, Rigaku MiniFlex600 with a Cu Kα source), Raman microscopy (Renishaw InVia confocal microscope with 633 nm laser source), Fourier-transform infrared spectroscopy (FTIR, Perkin Elmer Spectrum One), UV-vis spectroscopy (PerkinElmer Lambda 850), scanning electron microscopy (SEM, JEOL JSM-7610F Plus equipped with energy-dispersive X-ray spectroscopy, EDS), X-ray photoelectron spectroscopy (XPS, ULVAC-PHI 5000 VersaProbe III equipped with an Al Kα radiation), thermogravimetric analysis (Perkin Elmer TGA-4000), nitrogen adsorption/desorption analysis (Micromeritics ASAP 2060), and inductively coupled plasma mass spectrometry (ICP-MS, Perkin Elmer NexION 300X) were used to analyze the samples.

Electrochemical measurements.

The obtained manganese oxide was mixed with Super P and PVDF with a weight ratio of 7:2:1 in NMP solvent. The slurry was subsequently transferred onto carbon paper substrates with the typical mass loading of 1.2−1.4 mg cm^{-2}. The electrochemical performance was tested with CR2032 coin-type cells, made of the manganese oxide electrode, metallic zinc foil, and glass fiber separator. 1 M $ZnSO_4$ with 0.1 M $MnSO_4$ aqueous solution (80 μL) was used as the electrolyte unless specifically mentioned. The galvanostatic charge/discharge (GCD) cycles at 0.3, 1, 2, ,4, and 8 A g^{-1} were measured in the potential range of 1.0−1.9 V (vs. Zn^{2+}/Zn) using LAND CT2001A. The electrochemical impedance spectroscopic (EIS) analysis was measured at open circuit potential with the potential amplitude of 10 mV in the frequency range between 0.1 Hz and 100 kHz using CH Instruments 6273.

***In situ* electrochemical Raman measurements.**

The experimental setup and procedures followed our previous reports.[1-3] Typically, *in situ* Raman spectra were recorded by using 633 nm laser via a 50× objective lens (Leica) on the Raman microscope. The spectra were recorded at various potentials in the voltage range between 1.0 and 1.9 V, and each spectrum was obtained by pre-polarizing for 3 min and holding at the desired potential during the period of spectral acquisition.

***Ex situ* characterizations.**

For *ex situ* XRD and SEM characterizations, the manganese oxide electrodes were collected by dissembling coin-type cells and thoroughly washing with deionized water. The electrodes were dried in a vacuum oven without heating. The activation process (i.e., 25 GCD cycles between 1.0 and 1.9 V at 0.3 A g^{-1}) was applied for the manganese oxide electrodes before the ICP-MS tests. After the activation process, the electrodes were operated to the discharge state (1.0 V) or charged state (1.9 V). By dissembling

the coin-type cells, the Mn-containing solution was recovered by immersing the glass fiber separator in 1 mL deionized water. Next, the Mn concentration in the electrolyte was detected by ICP-MS. To avoid interference, 80 μL of 1 M $ZnSO_4$ aqueous solution was used as the electrolyte (without adding $MnSO_4$ additive) for the ICP-MS tests. The capacity contributions from one-electron (1e) and two-electron (2e) processes were estimated followed a previous report.[4] Firstly, the mass of active material undergoing 2e process (m_{2e}; mg) can be calculated by the difference in electrolyte Mn concentration between the discharged and charged states.

$$m_{2e} = \frac{(C_{Mn,dis} - C_{Mn,cha})}{54.94} \times V_e \times 86.94 \quad \text{(S1)}$$

where the $C_{Mn,dis}$ and $C_{Mn,cha}$ are the electrolyte Mn concentration at the discharged and charged states (ppm), respectively; V_e is the volume of electrolyte (L). The reversible 2e reaction capacity (C_{2e}; mAh) can be then obtained by multiplying by its theoretical capacity.

$$C_{2e} = m_{2e} \times 0.616 \quad \text{(S2)}$$

The 1e reaction capacity (C_{1e}; mAh) can be obtained by subtracting the 2e capacity from the overall capacity.

$$C_{1e} = C_{overall} - C_{2e} \quad \text{(S3)}$$

Accordingly, the mass of active material undergoing 1e process (m_{1e}; mg) can be converted by dividing with the theoretical capacity of 1e process.

$$m_{1e} = \frac{C_{1e}}{0.308} \quad \text{(S4)}$$

2. Supplementary figures

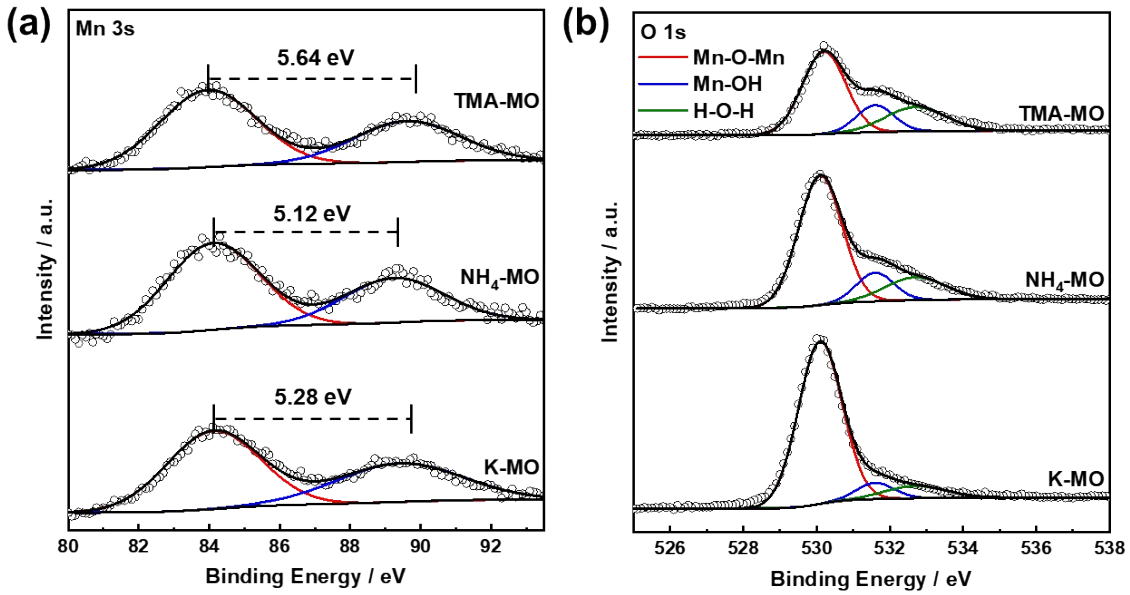

Figure S1. XPS (a) Mn 3s spectra, (b) O 1s spectra of K-MO, NH_4-MO, and TMA-MO.

As shown in **Figure S2a**, the K 2p spectrum of K-MO shows K $2p_{3/2}$ (292.9 eV) and K $2p_{1/2}$ (295.7 eV) signals, proving the presence of K^+ ions in the samples.[5] The N 1s spectrum of NH_4-MO shows a peak at 400.2 eV, which is the characteristic signal of NH_4^+ (**Figure S2b**).[6] Two peaks at 399.9 and 403.0 eV can be observed in the N 1s spectrum of TMA-MO, indicative of the existing TMA^+ ions in the sample.[7] Evidently, the above results confirm the successful incorporation of K^+, NH_4^+, and TMA^+ ions in the K-MO, NH_4-MO, and TMA-MO, respectively.

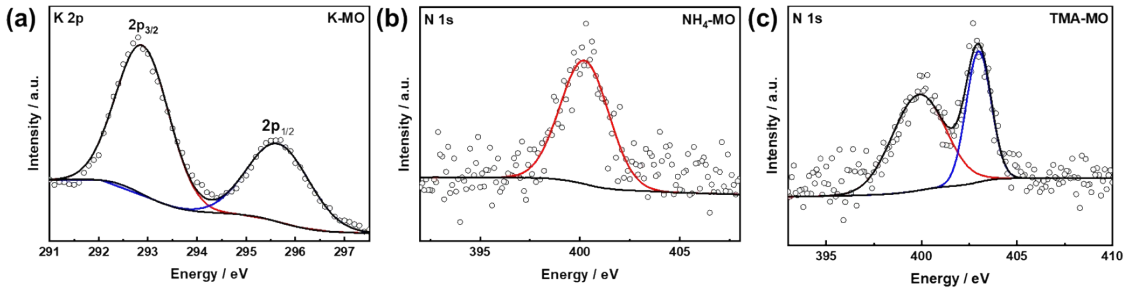

Figure S2. XPS (a) K 2p spectrum of K-MO, N 1s spectra of (b) NH_4-MO and (c) TMA-MO.

As shown in **Figure S3**, both air and N_2 flows were used to analyze the sample. The results show highly similar weight loss patterns when testing under air and N_2 flows. The weight loss below 100 °C is attributed to the physisorbed water originating from the ambient environment. The weight loss in the region between 100 and 200 °C corresponds to the structural water. The sharp decrease in the TMA-MO curve (even under N_2 flow) could be attributed to the decomposition of TMA^+ ions. Nevertheless, the structural water contents determined from air and N_2 flows are almost identical. For example, 7.3 and 7.4% were found for NH_4-MO by using air and N_2 flows, respectively. Accordingly, the reported structural water contents of the samples are based on the results measured under air flow (**Figure S4**).

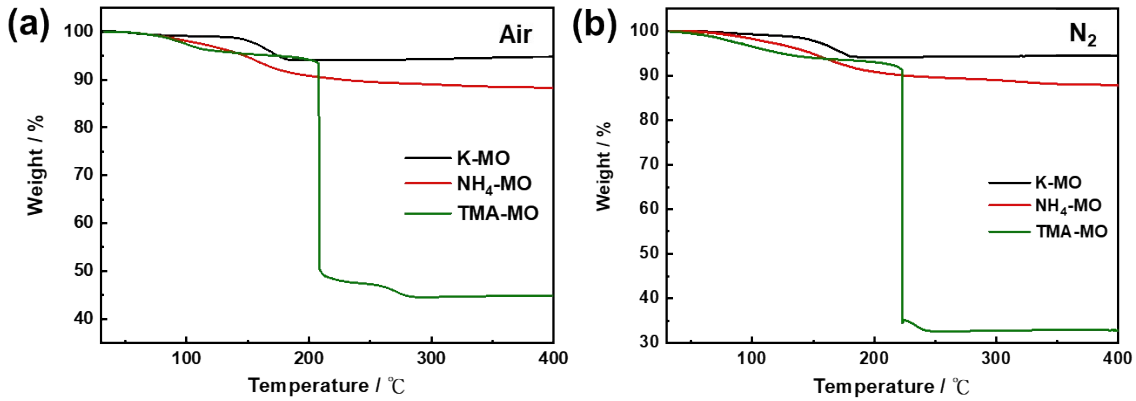

Figure S3. Weight loss curves of K-MO, NH_4-MO, and TMA-MO measured under (a) air and (b) N_2 flows.

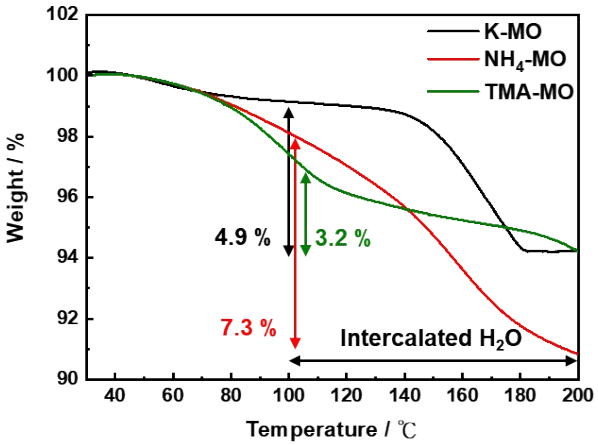

Figure S4. Enlarged weight loss curves of K-MO, NH_4-MO, and TMA-MO measured under air flow.

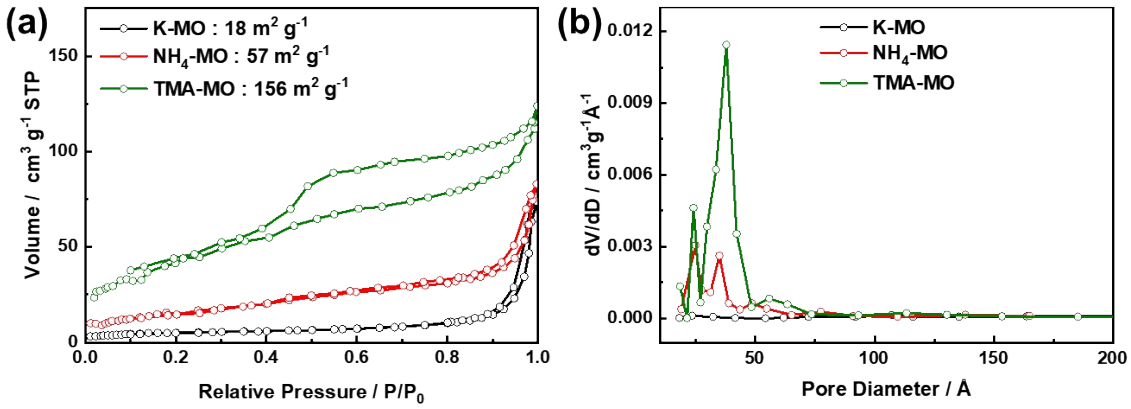

Figure S5. (a) nitrogen adsorption/desorption isotherms and (b) pore size distribution of K-MO, NH_4-MO, and TMA-MO.

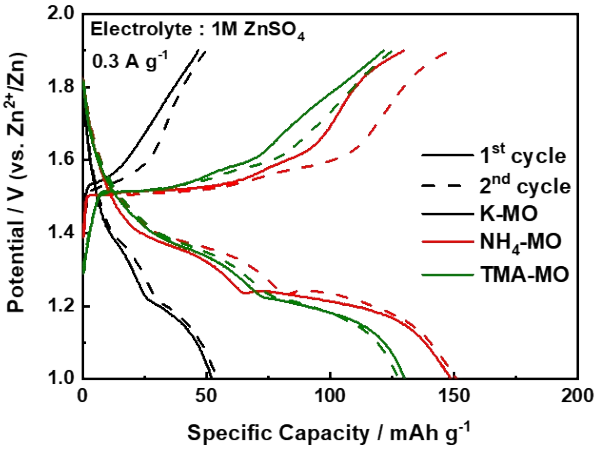

Figure S6. Initial two GCD cycles at 0.3 A g^{-1} of K-MO, NH_4-MO, and TMA-MO in 1 M $ZnSO_4$.

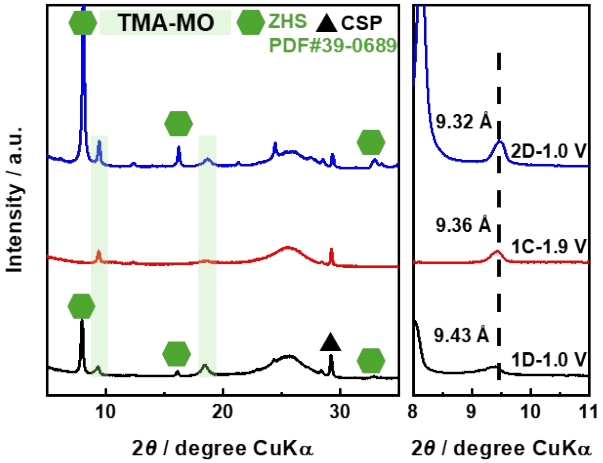

Figure S7. Selected *ex situ* XRD patterns of TMA-MO for the initial two cycles.

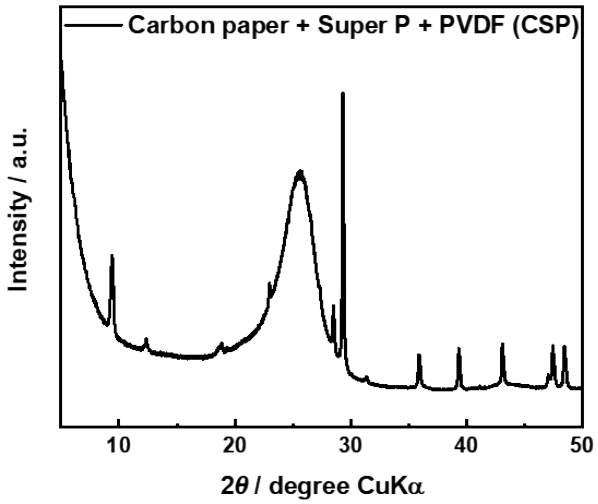

Figure S8. XRD pattern of carbon paper loaded with Super P and PVDF.

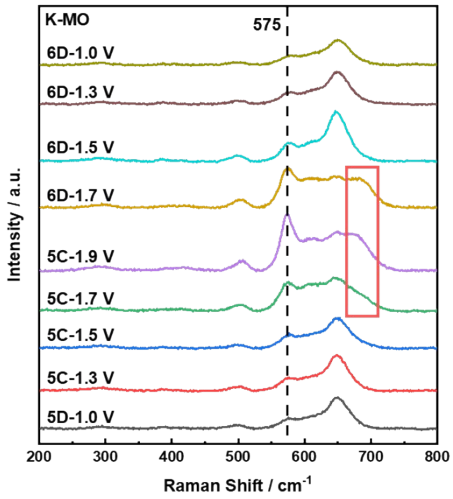

Figure S9. Selected *in situ* Raman spectra of K-MO for the 5th and 6th cycles.

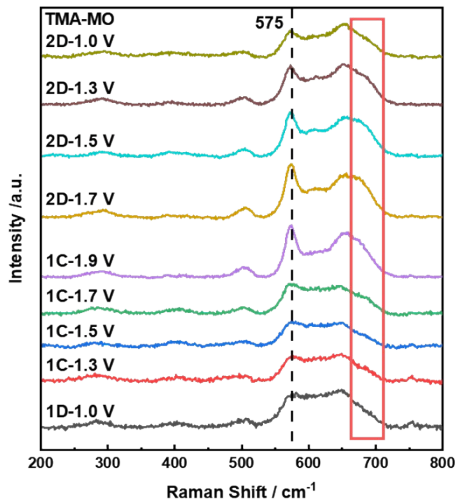

Figure S10. Selected *in situ* Raman spectra of TMA-MO for the initial two cycles.

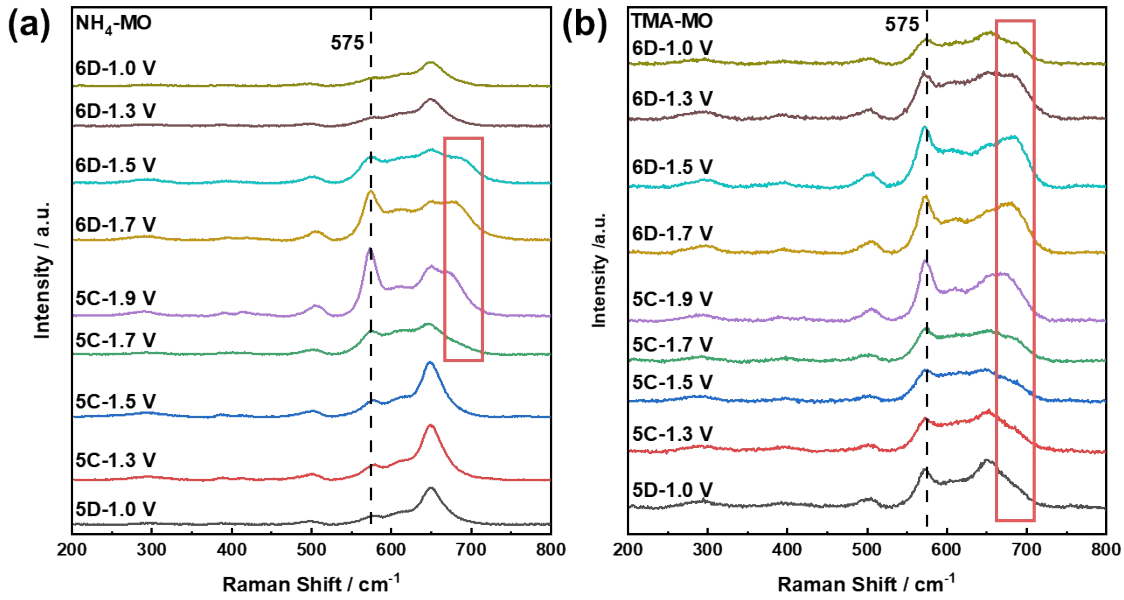

Figure S11. Selected *in situ* Raman spectra of (a) NH_4-MO and (b) TMA-MO for the 5th and 6th cycles.

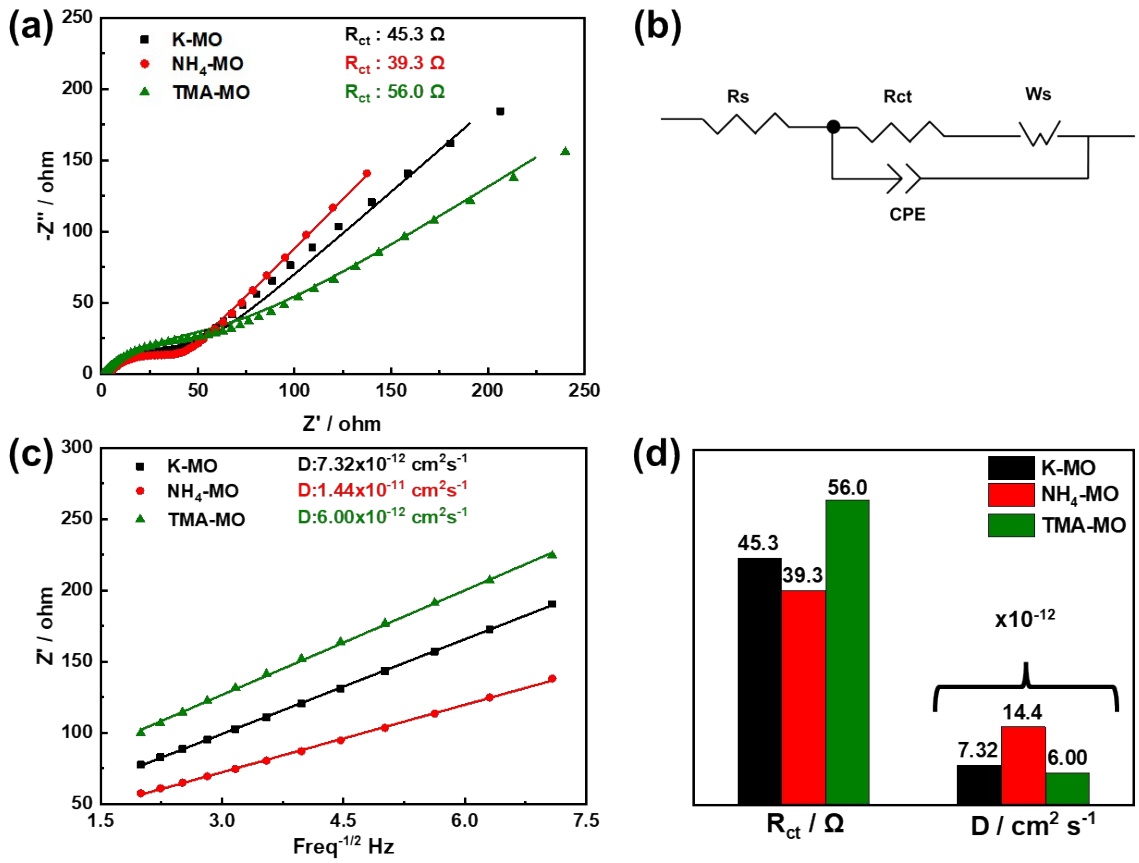

Figure S12. (a) EIS spectra, (b) equivalent-circuit model, (c) Z' vs. $\omega^{-0.5}$ plot, and (d) comparison of R_{ct} and D values of K-MO, NH_4-MO, and TMA-MO.

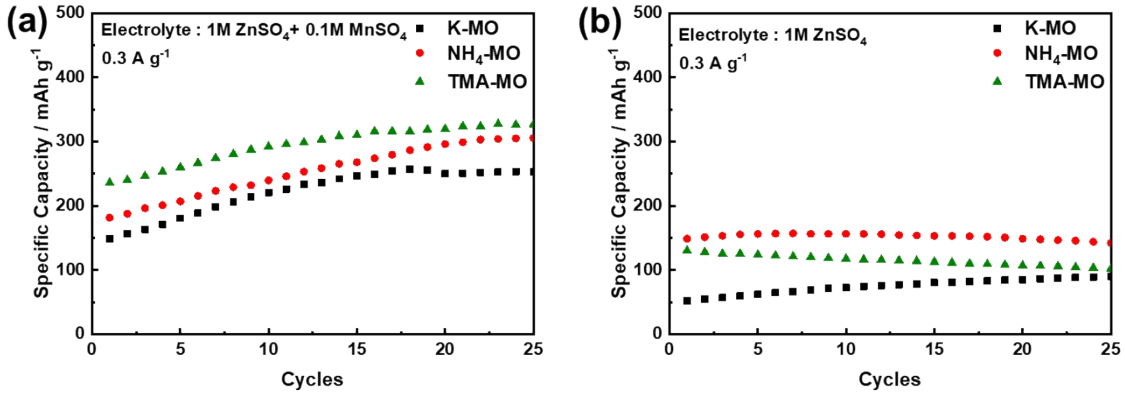

Figure S13. Cycle performance measured at 0.3 A g^{-1} of K-MO, NH_4-MO, and TMA-MO in 1 M $ZnSO_4$ (a) with and (b) without 0.1 M $MnSO_4$.

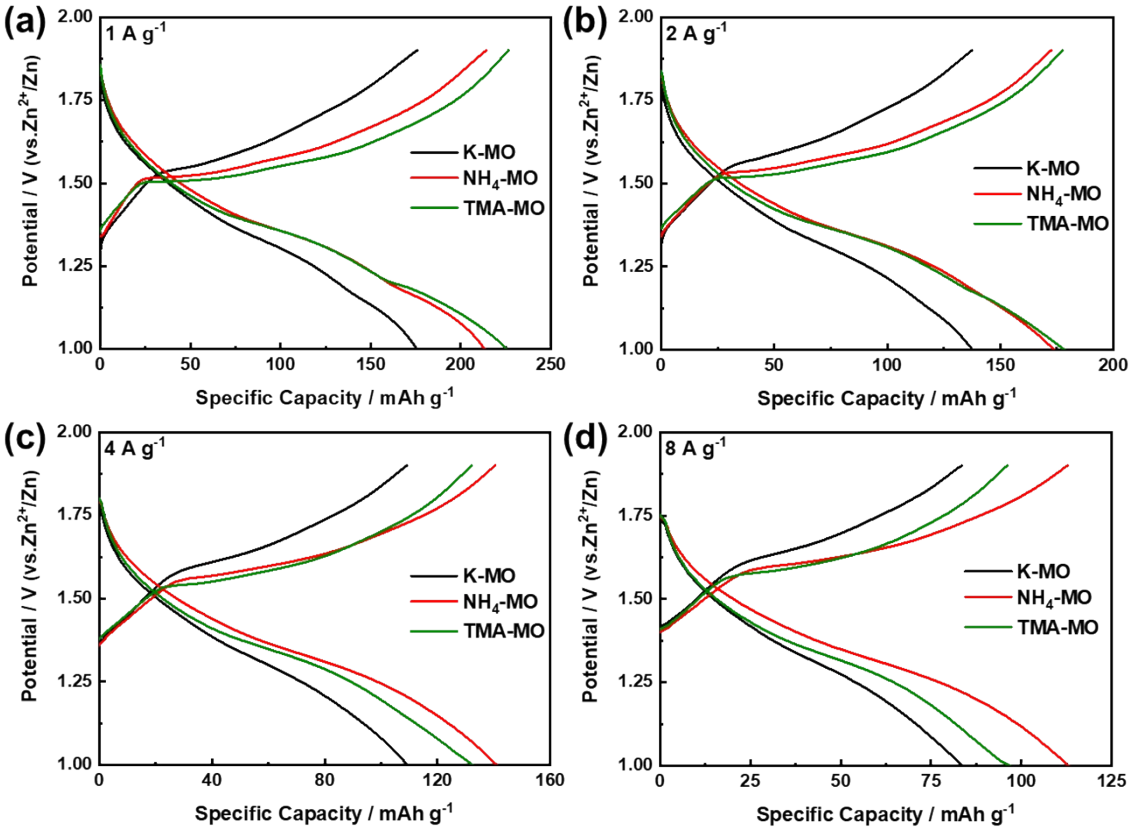

Figure S14. GCD curves recorded at (a) 1 A g^{-1}, (b) 2 A g^{-1}, (c) 4 A g^{-1}, and (d) 8 A g^{-1} of K-MO, NH_4-MO, and TMA-MO.

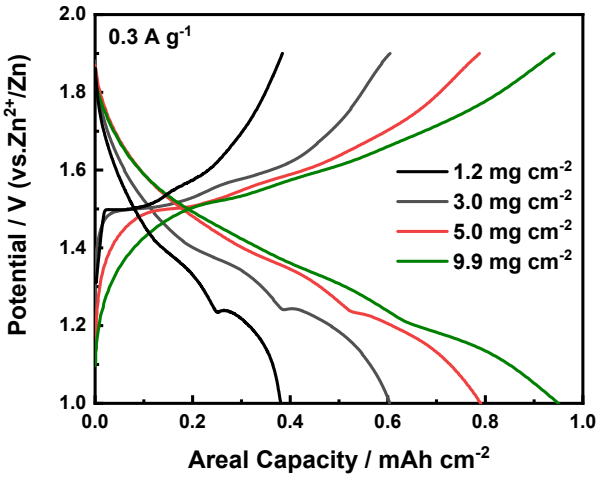

Figure S15. GCD curves at different loading masses of NH_4-MO.

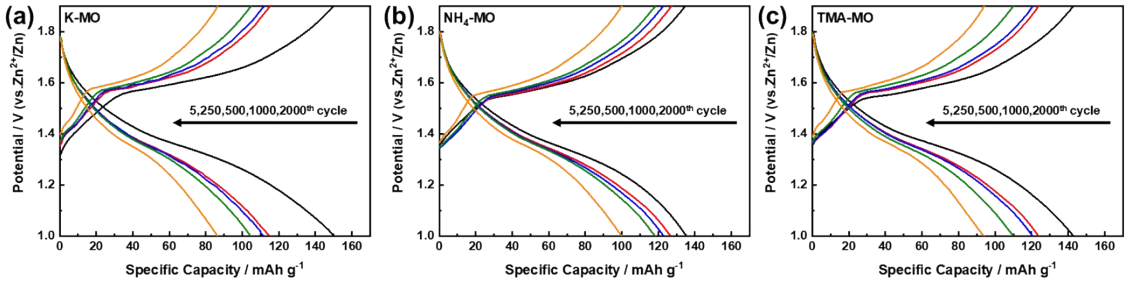

Figure S16. Selected GCD curves at 4 A g^{-1} over 2000 cycles of (a) K-MO, (b) NH_4-MO, and (c) TMA-MO

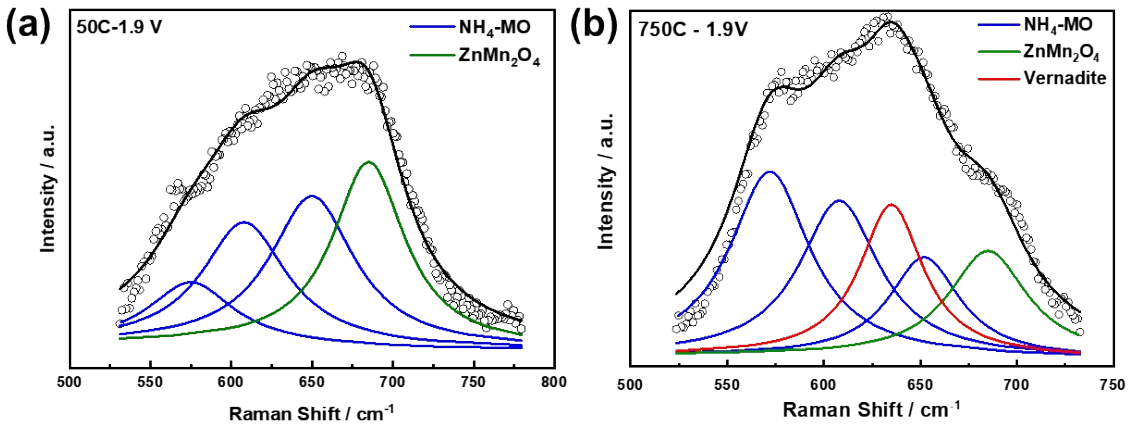

Figure S17. *Ex situ* Raman spectra of the NH_4-MO electrodes at the charged state (1.9 V) after (a) 50th cycle and (b) 750th cycle at 0.3 A g^{-1}.

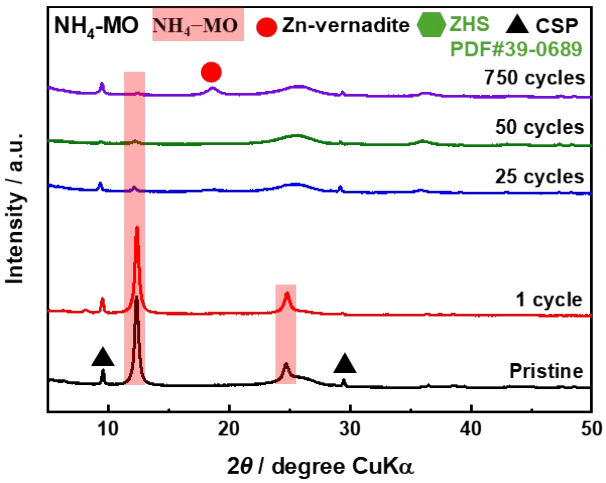

Figure S18. Selected *ex situ* XRD patterns of the NH_4-MO electrodes at the charged state (1.9 V) over 750 cycles at 0.3 A g^{-1}.

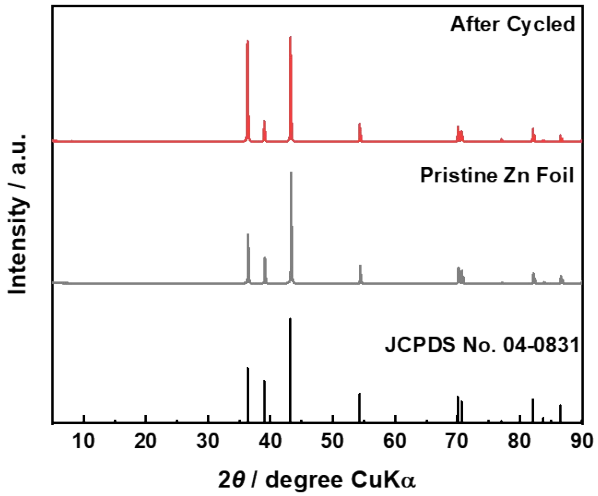

Figure S19. XRD patterns of pristine Zn foil and the Zn anode after 2000 cycles at 4 A g^{-1} from the Zn//NH_4-MO cell. The standard card of metallic Zn (JCPDS no. 04-0831) is added for comparison.

3. Supplementary Tables

Table S1 Characterization results of the prepared samples.

Sample	d_{001} (Å)	C/Mn[a]	Structural water (%)	Specific surface area ($m^2\ g^{-1}$)	Pore volume ($cm^3\ g^{-1}$)	Band gap (eV)
monoclinic K-MO	7.04	0.20	4.9	18	0.11	1.79
hexagonal NH_4-MO	7.18	0.12	7.3	57	0.12	1.54
hexagonal TMA-MO	9.43	0.20	3.2	156	0.18	2.34

[a] C = K, NH_4, or TMA

Table S2 Comparison table of battery performance of layered manganese oxides used in RAZIBs.

Cathode material	Electrolyte	Voltage window (V)	Discharge capacity (mAh g^{-1} / A g^{-1})	Specific capacity (mAh g^{-1})/ cycles/current density (A g^{-1})
NH_4-MnO_2 (NH_4-MO) this work	1 M $ZnSO_4$ 0.1 M $MnSO_4$	1.0−1.9	306@ 0.3 A g^{-1} 213 @ 1 A g^{-1} 113 @ 8 A g^{-1}	143/500/1 101/2000/4
TMA-MnO_2 (TMA-MO) this work	1 M $ZnSO_4$ 0.1 M $MnSO_4$	1.0−1.9	327 @ 0.3 A g^{-1} 225 @ 1 A g^{-1} 97 @ 8 A g^{-1}	117/500/1 90/2000/4
NH_4-MnO_2[8]	2 M $ZnSO_4$ 0.1 M $MnSO_4$	0.8−1.8	419 @ 0.5 A g^{-1} ~325 @ 1 A g^{-1} 56 @ 8 A g^{-1}	129/10000/4
NH_4-MnO_2[9]	2 M $ZnSO_4$ 0.1 M $MnSO_4$	0.8−1.8	229 @ 0.3 A g^{-1} 172 @ 1 A g^{-1} 123 @ 3 A g^{-1}	141/1500/2
NH_4F-MnO_2[6]	2 M $ZnSO_4$ 0.1 M $MnSO_4$	0.8−1.8	322 @ 0.1 A g^{-1} ~164 @ 0.3A g^{-1} ~140 @ 0.5 A g^{-1}	~50/1000/0.5
TMA-MnO_2[10]	2 M $ZnSO_4$ 0.2 M $MnSO_4$	1.0−1.9	310 @ 0.2 A g^{-1} 200 @ 1 A g^{-1}	~121/1000/2

			116 @ 2A g^{-1}	
K-MnO_2[11]	2 M $ZnSO_4$ 0.1 M $MnSO_4$	1−1.85	272 @ 0.3 A g^{-1} 220 @ 1 A g^{-1} 95 @ 3 A g^{-1}	64/1000/2
Mg-MnO_2[12]	2 M $ZnSO_4$ 0.1 M $MnSO_4$	1.0−1.8	385 @ 0.3 A g^{-1} 298 @ 1.5 A g^{-1} 172 @ 6 A g^{-1}	~80/1000/3
Cu-MnO_2[13]	1 M $ZnSO_4$ 0.1 M $MnSO_4$	1.0−1.9	236@ 0.5 A g^{-1} 191@ 1 A g^{-1} 95@ 8 A g^{-1}	96/1500/4
Y-MnO_2[2]	1 M $ZnSO_4$ 0.1 M $MnSO_4$	1.0−1.9	212@ 0.5 A g^{-1} 179@ 1 A g^{-1} 94@ 8 A g^{-1}	94/3000/4
Mo-MnO_2[14]	2 M $ZnSO_4$ 0.1 M $MnSO_4$	0.9−1.8	280 @ 0.4 A g^{-1} 207 @ 1 A g^{-1} 107 @ 3 A g^{-1}	159/1000/1
MnO_2/MXene[15]	2 M $ZnSO_4$ 0.1 M $MnSO_4$	0.8−1.8	315 @ 0.2 A g^{-1} 249 @ 1 A g^{-1} 149 @ 5 A g^{-1}	132/5000/5

4. References

1. T. H. Wu, Y. Q. Lin, Z. D. Althouse and N. Liu, *ACS Appl. Energy Mater.*, 2021, **4**, 12267.
2. T. H. Wu, Y. Q. Lin and J. X. Huang, *Nanoscale*, 2023, **15**, 1869.
3. T. H. Wu, T. K. Li and L. J. Guo, *J. Power Sources*, 2024, **623**, 235503.
4. Y. Liu, K. Wang, X. Yang, J. Liu, X. X. Liu and X. Sun, *ACS Nano*, 2023, **17**, 14792.
5. Y. Jiao, L. Kang, J. Berry-Gair, K. McColl, J. Li, H. Dong, H. Jiang, R. Wang, F. Corà, D. J. L. Brett, G. He and I. P. Parkin, *J. Mater. Chem. A*, 2020, **8**, 22075.
6. L. Yan, Y. Han, C. Zhu, L. Luo, Y. Qin, D. Yu, B. Liu, X. Zou, Y. Zhou and B. Xiang, *Nano Energy*, 2024, **122**, 109331.
7. F. Y. Cheng, C. H. Su, Y. S. Yang, C. S. Yeh, C. Y. Tsai, C. L. Wu, M. T. Wu and D. B. Shieh, *Biomaterials*, 2005, **26**, 729.
8. H. Yao, H. Yu, Y. Zheng, N. W. Li, S. Li, D. Luan, X. W. D. Lou and L. Yu, *Angew. Chem. Int. Ed.*, 2023, **62**, e202315257.
9. S. Wang, X. Zhao, H. Chen, J. Guo, R. Liu and D. a. Yang, *EcoMat*, 2022, **4**, e12249.
10. Z. Zhou, J. Tong, X. Zou, Y. Wang, Y. Bai, Y. Yang, Y. Li, C. Wang and S. Liu, *J. Mater. Chem. A*, 2024, **12**, 10923.
11. Q. Xie, G. Cheng, T. Xue, L. Huang, S. Chen, Y. Sun, M. Sun, H. Wang and L. Yu, *Mater. Today Energy*, 2022, **24**, 100934.
12. J. Xia, Y. Zhou, J. Zhang, T. Lu, W. Gong, D. Zhang, X. Wang and J. Di, *Small*, 2023, **19**, 2301906.
13. T. H. Wu, W. Y. Liang and Y. Q. Lin, *J. Taiwan Inst. Chem. Eng.*, 2022, **131**, 104172.
14. Z. Wang, K. Han, Q. Wan, Y. Fang, X. Qu and P. Li, *ACS Appl. Mater. Interfaces*, 2023, **15**, 859.
15. Y. Wang, L. Liu, Y. Wang, J. Qu, Y. Chen and J. Song, *ACS Nano*, 2023, **17**, 21761.